

*friction, wear, cutting,
silicon nitride ceramic tool,
spheroidal cast iron*

Wit GRZESIK¹
Krzysztof ZAK¹

ASSESSMENT OF FRICTION INCORPORATING TOOL WEAR EFFECT

This paper compares friction for orthogonal and non-orthogonal models developed for chamfered ceramic tools with a large negative rake angle. The new non-orthogonal friction model was tested for the machining of spheroidal cast iron (SCI) using coated nitride ceramic inserts. Friction coefficients were determined on the rake and flank face for fresh and worn ceramic inserts using the values of force components recorded during tool wear tests at different cutting speeds. In particular, the friction and normal forces acting on the rake and flank faces were computed. It was revealed that friction coefficients at the tool-chip and tool-workpiece interfaces change substantially with the tool wear progress and differ from that determined for orthogonal friction model.

1. INTRODUCTION

Friction has been one of the fundamental problems of machining research and modelling for over a hundred years. The present knowledge on friction in metal cutting is predominantly based on the orthogonal cutting model and Coulomb's law [1],[2]. As a result, it is insufficient to accurately model mechanistic, thermal and tribological phenomena. For instance [3], using input data relying on Coulomb's friction coefficient can generate more than 50% differences in cutting forces and the tool-chip contact length. It is evident that 3D models and simulations should be based on the oblique cutting using cutting tools with defined inclination angle λ_s [1]. Although the inclination angle for commercial turning tools is relatively small ($\lambda_s = -7^\circ$) its value for milling cutters, helical drills and broaching and shaving tools are in tens of degrees. The problem becomes complex when using ceramic and CBN cutting inserts with the negative rake angles of the chamfer of -20° or -30° , which protect cutting edges made of brittle materials against premature failure [1],[4]. It was revealed that the influence of both inclination and rake angles cause that the components of the resultant cutting force change distinctly in comparison to the orthogonal cutting. As a result, the friction at the contact parts of the cutting tool should be altered as well [5],[6]. This results from the fact that according to the Coulomb's rule the friction coefficients μ_γ and μ_α are defined as the ratios of the normal force and friction force acting

¹ Opole University of Technology, Faculty of Mechanical Engineering, Poland, E-mail: w.grzesik@po.opole.pl

respectively on the rake and flank faces [1],[2].

It has recently been documented by Grzesik et al. [7],[8] that for machining of spheroidal cast iron (SCI) with CBN tools, friction changes substantially during the evolution of tool wear. In general, in the oblique cutting, the mechanics of oblique cutting is considered in terms of the normal rake angle [1],[5],[9]. In consequence, the friction coefficient lower than 0.1 is often obtained because a high negative rake angle causes the normal force to increase and the friction force to decrease [6],[9]. Apart from mechanistic factors thermally controlled factors such as the sliding velocity also influence friction because it changes normal and shear loads on the working parts of the cutting tools [10],[12].

It was documented [7],[8] that in a non-orthogonal machining with worn CBN tools noticeably higher passive and feed forces occur which influence the tribological interactions at the rake face. This paper proposes a revised friction model for the turning with chamfered fresh and worn nitride ceramic (Si_3N_4) tools. In order to determine the friction coefficients the friction and normal forces acting on both rake and flank faces were discretely computed during several wear tests.

2. MODELLING OF FRICTION BASED ON CUTTING FORCES

2.1. RESOLVING OF THE RESULTANT CUTTING FORCE IN DIFFERENT COORDINATE SYSTEMS

Figure 1 presents the localizations of the reference planes, axes of the coordinate systems and the measured components of the resultant cutting force F . In addition Fig. 2 shows forces acting on the insert tip and forces acting on both rake and flank faces.

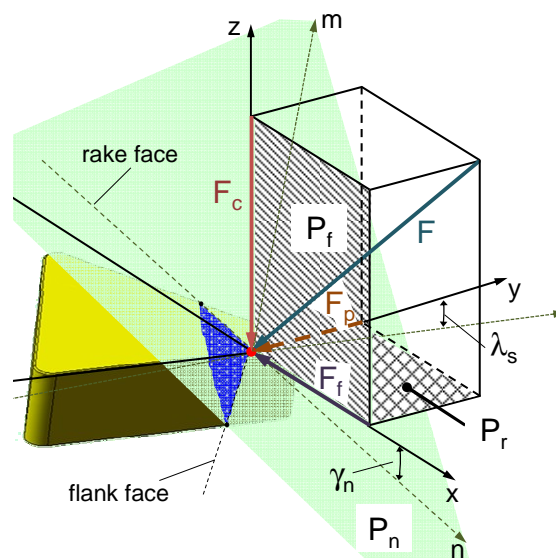


Fig. 1. Localization of reference planes and axes of coordinate systems

As shown in Fig. 1, the resultant force F is resolved in the xyz coordinate system into the three components- cutting force F_z , feed force F_x and passive (thrust) force F_y . Other three components- F_l , F_m and F_n components characteristic for non-orthogonal cutting act in the lmn coordinate system in which axis l is parallel and m - n plane is perpendicular to the cutting edge respectively [1,5]. By the geometrical summation of forces one obtains:

$$\bar{F} = \bar{F}_x + \bar{F}_y + \bar{F}_z = \bar{F}_l + \bar{F}_m + \bar{F}_n \quad (1)$$

Because the lmn system (Fig. 1) is obtained by the transformation of the xyz system using two subsequent rotations- firstly by the angle λ_s around the axis x and secondly around the axis y by the normal rake angle γ_n , the forces F_l , F_m and F_n can be calculated using the following matrix equation.

$$\begin{bmatrix} F_n \\ F_l \\ F_m \end{bmatrix} = [TM]_x [TM]_y \begin{bmatrix} F_x \\ F_y \\ F_z \end{bmatrix} = \begin{bmatrix} \cos \gamma_n & 0 & -\sin \gamma_n \\ -\sin \lambda_s \sin \gamma_n & \cos \lambda_s & -\sin \lambda_s \cos \gamma_n \\ \cos \lambda_s \sin \gamma_n & \sin \lambda_s & \cos \lambda_s \cos \gamma_n \end{bmatrix} \begin{bmatrix} F_x \\ F_y \\ F_z \end{bmatrix} \quad (2)$$

Equivalently to Eqn. (2), three equations which express components F_l , F_m and F_n in terms of the measured F_x , F_y and F_z forces are derived:

$$F_l = -F_x \sin \lambda_s \sin \gamma_n + F_y \cos \lambda_s - F_z \sin \lambda_s \cos \gamma_n \quad (3.1)$$

$$F_m = F_x \cos \lambda_s \sin \gamma_n + F_y \sin \lambda_s + F_z \cos \lambda_s \cos \gamma_n \quad (3.2)$$

$$F_n = F_x \cos \gamma_n - F_z \sin \gamma_n \quad (3.3)$$

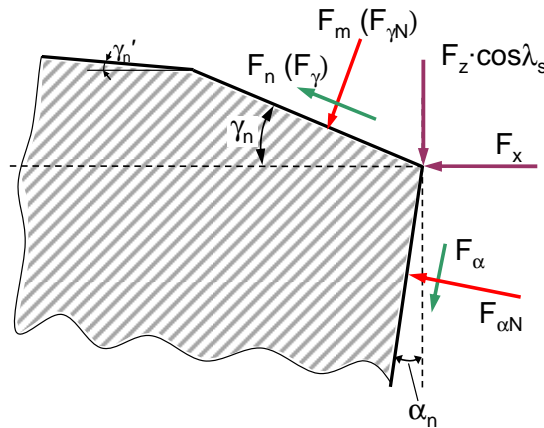


Fig. 2. Forces acting on the chamfer and flank face

According to the force resolution presented in Fig. 2 the friction force on the rake face is equal to the F_n component and the normal force is equal to the F_m component. Moreover, the friction and normal forces acting on the flank face are equal to:

$$F_{\alpha} = F_z \cos \alpha_n - F_x \sin \alpha_n \quad (4.1)$$

$$F_{\alpha N} = -F_z \sin \alpha_n + F_x \cos \alpha_n \quad (4.2)$$

It should be taken into account that considering the friction on the flank face is only possible when a small land is formed artificially by honing or naturally due to wear [12].

2.2. FRICTION FOR ORTHOGONAL AND NON-ORTHOGONAL CUTTING MODELS

Taking into account that the friction force on the rake face F_{γ}^{ob} is equal to F_n and the normal force $F_{\gamma N}^{ob}$ is equal to F_m the average friction coefficient on the rake face is determined from Eqn. (5.1). By analogy, if the friction and normal forces on the flank face are denoted by F_{α} and $F_{\alpha N}$, the appropriate friction coefficient is determined from Eqn. (5.2).

$$\mu_{\gamma ob} = \frac{F_{\gamma}^{ob}}{F_{\gamma N}^{ob}} = \frac{F_n}{F_m} \quad (5.1)$$

$$\mu_{\alpha ob} = \frac{F_{\alpha}}{F_{\alpha N}} \quad (5.2)$$

For orthogonal cutting, the friction coefficient is determined as [1]:

$$\mu_o = \operatorname{tg} \left[\operatorname{tg}^{-1} \left(\frac{F_z}{F_x} \right) + \gamma_o \right] \quad (6)$$

3. EXPERIMENTAL PROCEDURE

3.1. MACHINING DETAILS

Machining and wear tests were performed on the bars made of spheroidal cast iron, EN-GJS-500-7 grade [13], using a CNC turning center, model Somab Transmab 450TD. Ceramic Si_3N_4 cutting inserts coated with TiN layer, GC1690 grade by Sandvik Coromant, were selected. TNGA 16 04 08T02520 GC1690 inserts were clamped in PTNGR 2020 – 16 tool holder. The optical image of the insert corner and SEM image of the worn tool nose are presented in Fig. 3.

Nominal effective rake angle was equal to $\gamma_{oe} = -6^\circ$, the chamfer angle was equal to $\gamma_{nc} = -20^\circ$ (the effective rake angle at the chamfer was $\gamma_{nce} = -26^\circ$) and the tool cutting edge angle $\kappa_r = 90^\circ$. The machining tests were carried out using a constant depth of cut $a_p = 0.8\text{mm}$ and the feed rate of 0.08mm/rev , and six variable cutting speeds of 100, 160, 240, 320, 400

and 480m/min. It should be noticed that a small feed rate of 0.08 mm/rev and chamfer width of 0.2mm were selected to concentrate the chip-rake contact on the chamfer area. This assumption allows relating all calculations of forces acting on the rake face to the chamfer angle (in Eqns. 3.1-3.3 $\gamma_n = \gamma_{nce}$).

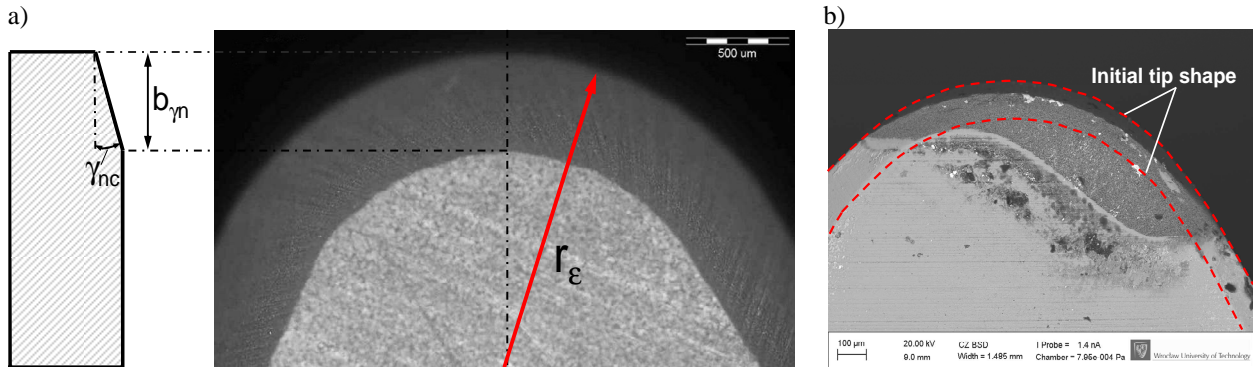


Fig. 3. Geometry of the cutting tool insert used-tool nose radius $r_{\epsilon}=0.8\text{mm}$, chamfer width $b_{\gamma n}=0.20\text{mm}$, rake angle $\gamma_{nc}=20^{\circ}$: a) fresh and worn, b) inserts

3.2. MEASUREMENTS OF FORCES AND THE TOOL WEAR

F_z , F_y and F_x components of the resultant cutting force (Fig. 1) were measured using a Kistler 9257A piezoelectric dynamometer and a Kistler 5070 signal amplifier to amplify the generated force signals. The measured data were recorded using a DasyLab v9.0 data acquisition program. Wear scars on the flank face were measured on a Leica optical microscope equipped with a CCD camera and processed using an IM1000 program. Worn corners were examined using a Hitachi S-3400N SEM microscope.

4. EXPERIMENTAL RESULTS AND DISCUSSION

4.1. ASSESSMENT OF THE TOOL WEAR

Assessment of the tool wear was based on measurements of the nose wear VB_C . Its discrete values were measured in a post-process mode keeping the time intervals between several to dozens of seconds. As a result, the wear curves corresponding to variable cutting speeds were drawn. The critical value of nose wear VB_C was set up at about 0.3mm. A SEM image of the Si_3N_4 tip with a marked VB_C wear indicator is presented in Fig. 4.

For instance, Fig. 4a shows the configuration of worn TiN/ Si_3N_4 tip after cutting test performed with the cutting speed of 400m/min. The topography of the worn corner was obtained using CLS microscope. By using appropriate graphical programs and different

rendering techniques it is possible to obtain any desired cross-section and the configuration of worn cutting wedge. Optionally, the configuration of the worn rake face can be recorded using SEM technique, as for instance in Fig. 4b.

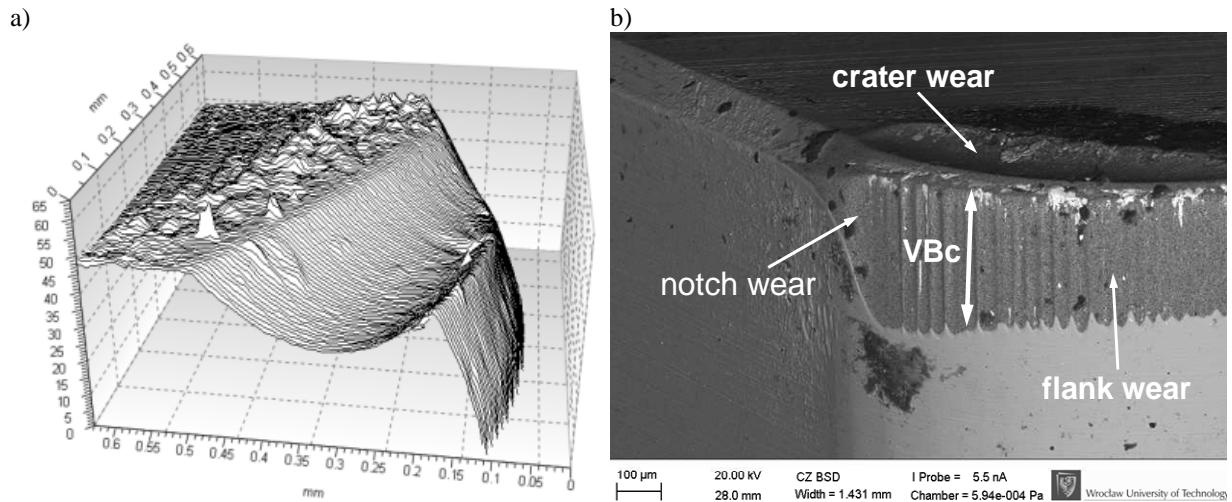


Fig. 4. Examples of 3D visualization of tool wear using confocal laser scanning (a) and SEM (b) techniques

As shown in Figs. 4 a and b the crater wear is developed on the chamfered rake face which, in turn, changes tribological conditions in comparison to the initial ones. Fig. 4 shows the progress of the flank wear depending on the cutting speeds selected in the wear tests. It is evident in Fig. 4 that the duration of the wear test, i.e. time to obtain the critical value of VB_C wear indicator is a function of the cutting speed used. Anyway, the tool life is rather short and for the medium cutting speed of 240m/min it is about 6.5min (equivalent cutting length is about 500m).

4.2. INFLUENCE OF TOOL WEAR ON FORCES

The changes of three directly measured components F_z , F_y and F_x of the resultant cutting force F during wear tests at the cutting speed of 240 and 480m/min are presented in Fig. 5a and b. Also the wear evolution is presented in Fig. 5.

At the beginning of wear test the cutting force F_z indicates a visible peak and further it increases depending on the cutting speed used. For both cutting speeds the values of F_z force at the end of all wear tests are equal to about 600N. According to Fig. 5, the feed force first increases, similarly to the F_z force, and after a shorter or longer stable stage its values decrease at the end of the wear tests. The thrust (passive) force F_y increases progressively. This fact evidently confirms that the wear process causes that the cutting performed with the chamfered Si_3N_4 ceramic and CBN tools can be considered as the non-orthogonal (oblique) cutting.

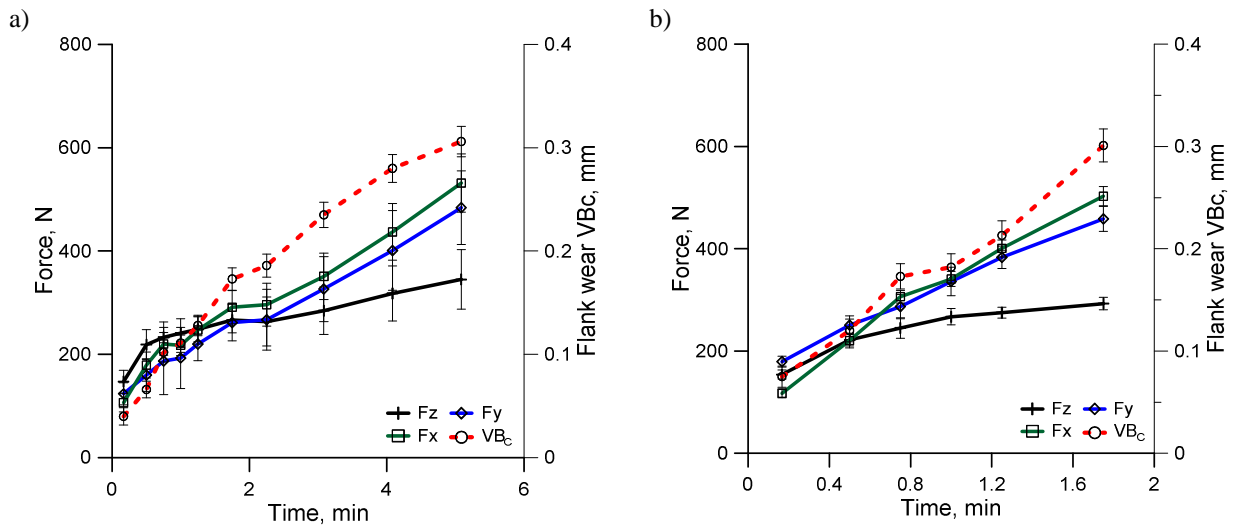


Fig. 5. Variation of componential cutting forces with progression of flank wear for: a) $v_c = 240$ m/min, b) $v_c = 480$ m/min ($f = 0.08$ mm/rev and $a_p = 0.8$ mm)

4.3. DETERMINATION OF FORCES ACTING ON THE RAKE AND FLANK FACES

The values of friction and normal forces acting on the chamfer with the rake angle of $\gamma_{nc} = -26^\circ$ determined for different wear state of the cutting inserts are presented in Fig. 6. Fig. 6 shows that courses and values of the friction and normal forces acting on the chamfer depend on the cutting speed used and the wear progress. In particular, they are distinctly higher when the cutting speed increases above 240 m/min and increase rapidly during a short time. For cutting speeds lower than 320 m/min, a small peak probably corresponding to the local failure of the TiN coating, was recorded at about 2nd min of the test.

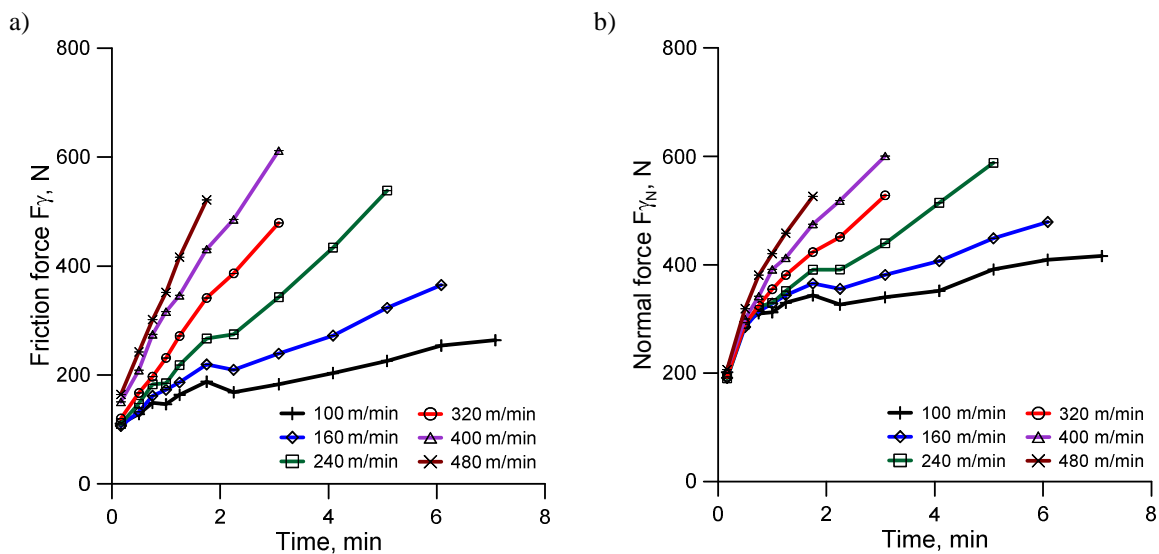


Fig. 6. Changes of friction (a) and normal (b) forces acting on the rake face during wear test

It can be observed in Fig. 6 that the normal forces change in a similar way. It is well known that normal loads exerted on an unworn chamfer do not depend on the cutting speed used but they depend on the feed rate used [12]. Because at a higher cutting speed the normal forces are comparable to the friction forces, the values of friction coefficient can approach 1.

This phenomenon occurs more visibly for higher cutting speeds of 400 and 480 m/min when wear develops during a shorter time. Based on the variations of friction and normal forces observed in this study two groups of wear mode can be distinguished, i.e. with or without a drop in forces at the first stage of the wear test. This tribological action of a thin TiN coating during the running-in period occur mostly for TiN coated CBN tools [14].

Fig. 7 shows changes of the friction and normal forces acting on the flank face due to its wear. It should be noticed that the normal force on the flank face (Fig. 7b) changes in a similar way as in Fig. 6b, although its values are lower. On the other hand, the friction force is practically independent of the cutting speed used.

This comparison suggests that the friction coefficient can distinctly exceed 1 at lower cutting speeds, which is a common case in the tribology of metal cutting process. For instance, it is reported that due to severe adhesion between the flank face and the fresh machined surface the value of μ_{α} is 1-1.4 [15],[16].

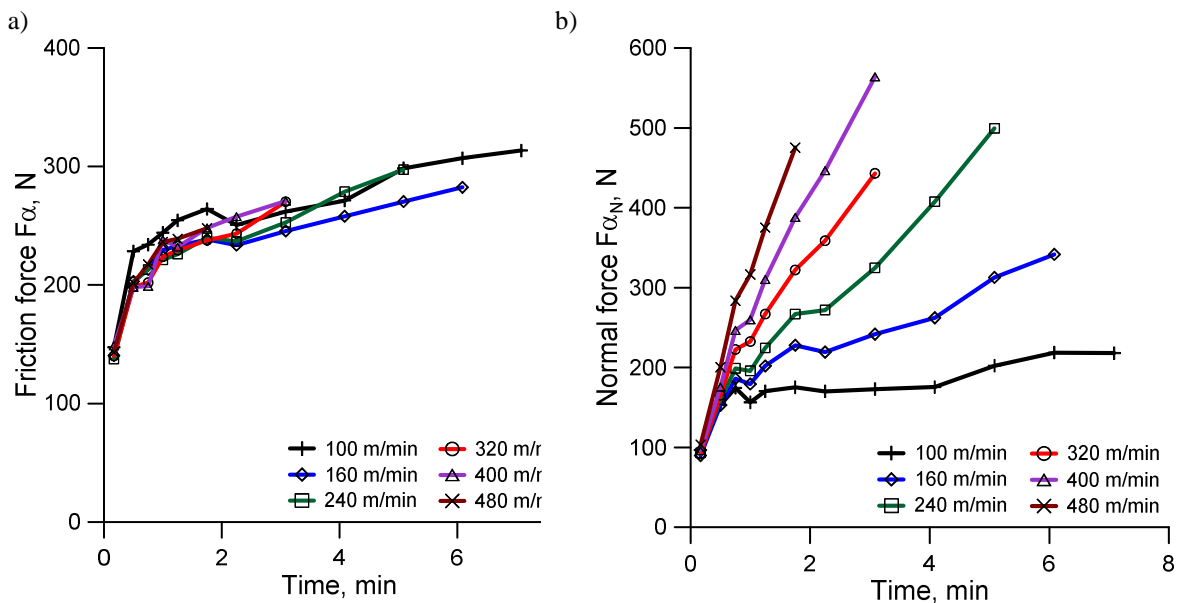


Fig. 7. Changes of friction (a) and normal (b) forces acting on the flank face during wear test

The cutting temperature of 400°-500°C characteristic for machining SCI with ceramic tools is suitable for the occurrence of severe adhesion at the flank face. The adhesion interaction is strengthened when TiN coating is rapidly removed from the Si_3N_4 substrate at higher cutting speeds. This scenario corresponds well to changes of the friction coefficient at the flank face presented in Fig. 9.

4.4. DETERMINATION OF FRICTION COEFFICIENTS AT RAKE AND FLANK FACES

Figure 8a presents the relevant changes of the friction coefficient $\mu_{\gamma_{ob}}$ obtained during the wear tests of Si_3N_4 tips for selected cutting speeds. Moreover, Fig. 8b shows relevant changes of $\mu_{\alpha_{ob}}$ on the flank face determined by Eqn. (5.2).

The data presented in Fig. 8 confirm that the coefficient of friction is sensitive to the cutting speed variations and the corresponding tool wear gradient. In general, during wear tests μ_{ob} oscillates between 0.45 and 1.0. A local minimum of μ observed at about 30 sec of the wear test in all wear trials corresponds to small BUE formed on the chamfer. The minimum values of μ_o and μ_{ob} are about 0.2 and 0.45 respectively. Differences between values of the friction coefficient obtained for fresh (unworn) cutting edges can be related to different normal loads determined by the two mechanical models considered.

The first peak of μ corresponds to the removal of the thin TiN coating during the running-in period but this effect is continuously reduced when the cutting (sliding) speed increases. At the cutting speed of 480 m/min this effect disappears because the TiN is removed very fast.

Similar variations of the coefficient of friction for ceramic materials are documented in Ref. [14]. In particular, the reduction of μ with the wear progresses can be related to the thermal softening enhancing at the temperature above 400-500°C. In the machining of SCI with the cutting speed of 240-480m/min, the measured maximum interface temperature ranges from about 450°C to 520°C and this effect is highly feasible [16].

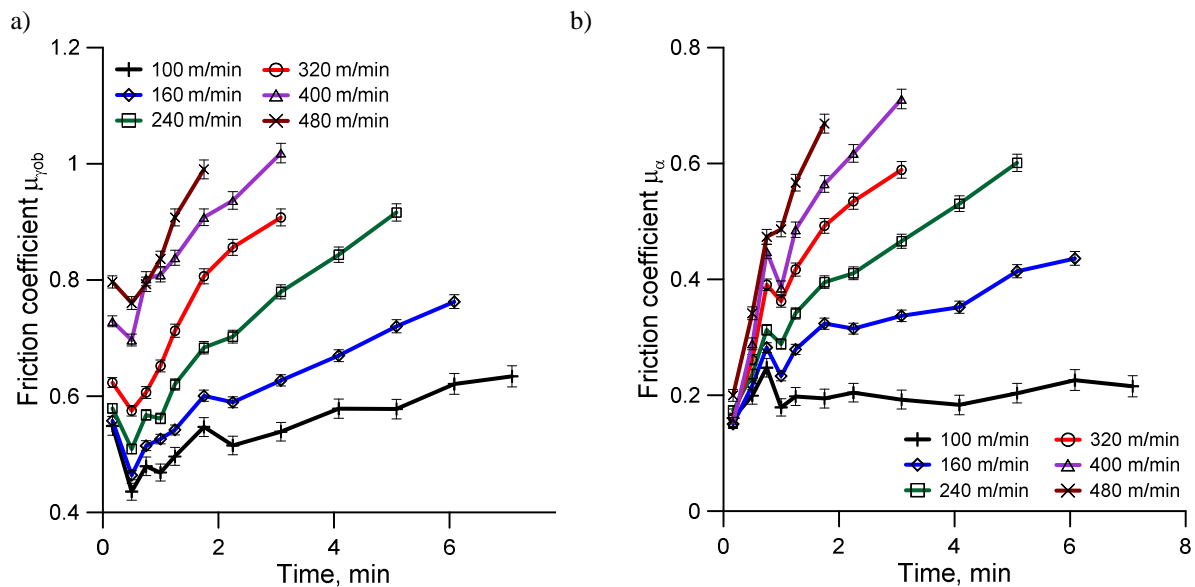


Fig. 8. Changes of friction coefficient at the rake (a) and flank (b) faces during wear tests

The differences in the values of $\mu_{\alpha_{ob}}$ obtained at a progressively increasing cutting speed are presented in Fig. 8b. At the lowest cutting speed of 100m/min the friction

coefficient is practically constant during the wear test due to the fact that TiN coating was not removed and it acts as an anti-adhesion barrier. With the increase of cutting speed the contact temperature increases and due to rapid coating removal severe adhesion between the silicon nitride ceramic and the SCI workpiece is activated [16]. As a result, at the highest cutting speeds of 400 and 480m/min the values of $\mu_{\alpha ob}$ approach even 2 (see also Fig. 9b).

The general comparison of the values of the three coefficients of friction - $\mu_{\gamma o}$, $\mu_{\gamma ob}$ and μ_{α} determined for fresh tools is shown in Fig. 9a. It is evident in Fig. 9a that the values of friction coefficients at the rake face - $\mu_{\gamma o}$ and $\mu_{\gamma ob}$ differ distinctly (at higher cutting speeds values of $\mu_{\gamma ob}$ are about four times higher). It should be noted in Fig. 9a that at the beginning of wear tests values of $\mu_{\gamma o}$ are practically independent of the cutting speed used. On the other hand, a similar behaviour of $\mu_{\gamma ob}$ take places at cutting speeds lower than 320m/min. It is interesting to note that for fresh tools the values of friction coefficients determined for rake and flank faces are comparable (differences in the same cases are of about 0.1).

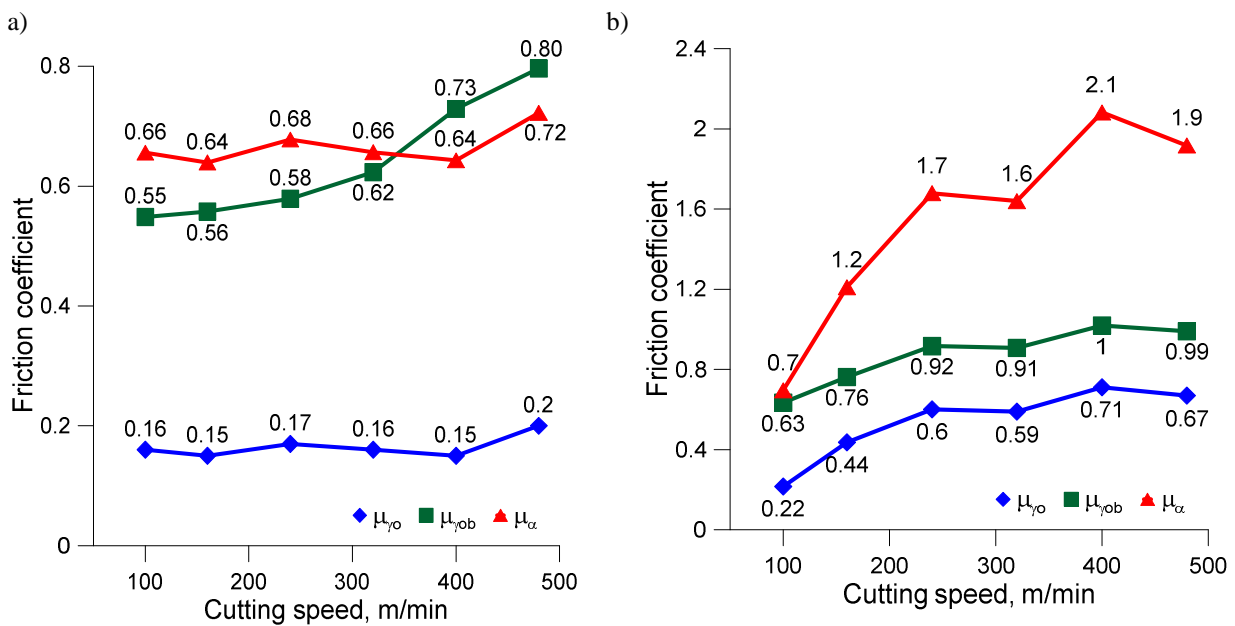


Fig. 9. Comparison of μ values obtained for orthogonal and oblique cutting models for cutting insert: a) fresh, b) worn

As shown in Fig. 9b, friction coefficients on the rake and flank faces increase with the wear progress and their values are higher in comparison to the result obtained for fresh tools. It can be noted that for the highest cutting speed the values of $\mu_{\gamma ob}$ approach 1. In particular substantial differences between μ_{α} and $\mu_{\gamma ob}$ resulting from wear progress can be seen in Fig. 9b. At the end of the wear test performed with high cutting speeds the values of μ_{α} are about 2, whereas the values of $\mu_{\gamma ob}$ approach 1. This fact evidently indicates different tribological behaviour of the rake and flank faces during tool wear.

5. CONCLUSIONS

1. The proposed methodology allows determining the values of the friction coefficient at the rake and flank faces for a selected time during the wear test.
2. Substantial differences between values of friction coefficient determined for orthogonal and non-orthogonal cutting were revealed. They are higher for fresh tools and lower for worn tools.
3. Differences between values of μ for orthogonal and non-orthogonal friction models are due to the overestimation of normal loads assessed for the orthogonal friction model.
4. Values of friction coefficient for the rake and flank faces are practically the same for fresh tools but differ substantially when tool wear progresses. They can approach values of 1 and 2 respectively which suggests severe adhesion at the flank face.

REFERENCES

- [1] GRZESIK W., 2008, *Advanced machining processes of metallic materials*, Elsevier, Amsterdam.
- [2] SHAW M.-C., 1989, *Metal cutting principles*, Clarendon Press, Oxford.
- [3] ÖZEL T., 2006, *The influence of friction models on finite element simulations of machining*, Int. J. Mach. Tools Manuf., 46, 518-530.
- [4] ZHOU J. M., WALTER H., ANDERSSON M., STAHL J. E., 2003, *Effect of chamfer angle on wear of PCBN cutting tool*, Int. J. Mach. Tools Manuf., 43, 301-305.
- [5] GRZESIK W., 1990, *The mechanics of continuous chip formation in oblique cutting with single-edged tool –Part I. Theory*, Int. J. Mach. Tools Manuf., 30, 359-371.
- [6] GRZESIK W., 1990, *The mechanics of continuous chip formation in oblique cutting with single-edged tool –Part II. Experimental verification of the theory*, Int. J. Mach. Tools Manuf., 30, 373-388.
- [7] GRZESIK W., ŻAK K., 2013, *Friction quantification in the oblique cutting with CBN chamfered tools*, Wear, 304, 36-42.
- [8] GRZESIK W., KOWALCZYK D., ŻAK K., 2013, *A new mechanistic friction model for the oblique cutting with tool wear effect*, Trib. Int., 66, 49-53.
- [9] KOMANDURI R., LEE M., RAFF L.-M., 2004, *The significance of normal rake in oblique cutting*, Int. J. Mach. Tools Manuf., 44, 1115-1124.
- [10] ZEMZENI F., RECH J., BEN SALEM W., DOGUI A., KAPSA P., 2009, *Identification of a friction model at tool/chip/workpiece interface in dry machining of AISI4142 treated steels*, J. Mater. Proc. Technol., 209, 3978-3990.
- [11] GRZESIK W., 1999, *Experimental investigation of the influence of adhesion on the frictional conditions in the cutting process*, Trib. Int., 32, 15-23.
- [12] POLETIKA M.F., 1969, *Contact loads on the active parts of cutting tools*, Mašinstroenie, Moscow, (in Russian).
- [13] GRZESIK W., KISZKA P., KOWALCZYK D., RECH J., CLAUDIN CH., 2012, *Machining of nodular cast iron (PF-NCI) using CBN tools*, Proc. 4th HPC Conf., Zurich, Procedia CIRP, 1, 500–504.
- [14] HOLMBERG K., MATTHEWS A., 1998, *Coating tribology*, Elsevier, Amsterdam.
- [15] GRZESIK W., MAŁECKA J., 2011, *Documentation of tool wear progress in the machining of nodular ductile iron with silicon nitride-based tools*, CIRP Annals. Manuf. Technol., 60/1, 121-124.
- [16] GRZESIK W., ZALISZ Z., NIESŁONY P., 2002, *Friction and wear testing of multilayer coatings on carbide substrates for dry machining applications*, Surf. Coat. Technol., 155, 37-45.